ChemPubSoc Europe

DOI: 10.1002/batt.201900081

BATTERIES & SUPERCAPS
Articles

New Insights into Nail Penetration of Li-Ion Batteries: Effects of Heterogeneous Contact Resistance

Meijie Chen[+],[a, b] Qin Ye[+],[a] Changmin Shi,[a] Qian Cheng,[a] Boyu Qie,[a] Xiangbiao Liao,[a] Haowei Zhai,[a] Yurong He,[b] and Yuan Yang*[a]

Nail penetration is one important mode of catastrophic failure in Li-ion batteries, and the contact resistance between a nail and electrodes is a dominant factor for heat generation. Surprisingly, previous studies always assume uniform resistance and there is no experimental measurement of contact resistance, to the best of our knowledge. In this report, the contact resistance is determined experimentally. The contact resistance between a nail (diameter = 1.25 mm) and a Cu/graphite electrode is $2.5 \pm 1.5\ \Omega$, and a nail and Al/$LiCoO_2$ is $20.3 \pm 12.4\ \Omega$. These values are in the same order of the geometric mean of the resistance between nail/metal substrate and nail/active materials, suggesting a random connection network among the nail, the metal substrate, and active materials. It is found that the resistance can vary as large as 1–2 orders of magnitude, and such fluctuation is critical to the magnitude of temperature rise during nail penetration, which can increase temperature rise by ~93% compared to homogeneous contact resistance. The results show that the heterogeneity in contact resistance should be considered. Based on such new understanding, a simple approach to reduce the temperature increase during nail penetration was proposed by having the anode as the outermost layer.

1. Introduction

Rechargeable Li-ion batteries are critical to various applications, such as portable electronics, vehicle electrification and grid-level energy storage.[1–3] However, Li-ion batteries have low thermal stability and can explode when they are exposed to abusive conditions such as mechanical deformation, short circuit, over-charging and external heating.[4–6] Such instability originates from the high flammability of organic electrolyte and becomes more severe upon the pursuit of batteries with high energy density.[7–8,9] Among various kinds of abuse, internal short-circuit is common and one of the most dangerous failure modes, which leads to excessive local heating to hundreds of degree Celsius and thermal runaway.[10,11] Extensive studies have been applied to avoid such thermal runaway. For example, thermal switches have been reported based on thermoresponsive polymeric materials,[12,13] and a bifunctional separator was used for early detection of internal shorting.[14] On the other hand, fundamental understanding is still needed to unveil this complicated electrochemical-thermal-electrical coupled process. Various advanced tools have been used to study Li dendrite growth mechanism and design principles for dendrite-free Li metal batteries, such as optical microscopy,[15] electron microscopy,[16–17,18] nuclear magnetic resonance (NMR),[19] Raman[20] and Synchrotron.[21] Nail penetration test is widely employed for evaluating thermal runaway after internal short circuits, as it is the most aggressive way to induce internal shorting.[22–24] Yokoshima et al. used X-ray inspection to directly observe the smoke generation inside and around a battery cell, ballooning of the pouch, as well as structural evolution of electrode materials in real time.[25] Kim et al. investigated the internal short circuit of a lithium polymer battery by infrared measurement during nail penetration.[26] Liu et al. studied different electrochemical behaviors of internal short circuit using a highly reproducible mechanical penetration method.[27] Various simulations were conducted to investigate thermal behaviors of batteries under nailing.[28–32] These studies indicate that the heat generation is localized at the contact between a nail and battery electrodes, and the electronic contact resistance (R_c) at nail/electrode interface is a dominant factor for the magnitude of local heat generation and the maximum temperature increase, which directly affects whether thermal runaway and explosion occur or not.[33–35] When the contact resistance is the same as the internal resistance of the battery, the temperature rise can reach as high as ~670 °C theoretically, which greatly exceed the thermal runaway temperature.[36]

Given the importance of contact resistance, it is critical to understanding its value and distribution in real scenarios. However, the authors are not aware of any experimental measurement of R_c in literature. Previous simulations simply assume a constant R_c for all contacts to simplify the model. Obviously R_c could vary from layer to layer, and there is no study to consider the effect of such heterogeneity and how such distribution depends on various factors such as properties of nail and metals/electrodes. The specific roles of electrode

[a] M. Chen,[+] Q. Ye,[+] C. Shi, Dr. Q. Cheng, B. Qie, X. Liao, H. Zhai, Prof. Y. Yang
Department of Applied Physics and Applied Mathematics
Columbia University
New York, NY 10025, USA
E-mail: yy2664@columbia.edu
[b] M. Chen,[+] Prof. Y. He
School of Energy Science & Engineering
Harbin Institute of Technology
Harbin 150001, P. R. China
[+] These authors contributed equally to this work.

Supporting information for this article is available on the WWW under https://doi.org/10.1002/batt.201900081

materials and current collectors in R_c are also unclear. In this report, we first build an electrochemical-thermal coupled model to understand the effect of the heterogeneity on R_c, followed by experimental determination of R_c and its dependence on electrodes, electrolytes, metal substrates and other factors. We find that the contact resistance can vary by a factor of more than 10 and such heterogeneity can cause ~93% higher temperature rise. These results illustrate the importance to take such factor into account in safety design of batteries. Such understanding also leads an optimized configuration with reduced heat generation in nail penetration.

2. Results and Discussion

2.1. Simulation on Effects of Heterogeneous R_c

First, to better understand the effect of heterogeneous R_c on the temperature increase during nail penetration, we build an electrochemical-thermal coupled short circuit model based on a $LiCoO_2$/graphite pouch cell with two repeating units (Figure 1a). The sequence is Cu (6)/graphite (60)/separator (30)/$LiCoO_2$ (40)/Al (6)/$LiCoO_2$ (40)/separator (30)/graphite (60)/Cu (6), where numbers in parentheses are corresponding thicknesses with the unit of μm. A nail with a diameter (D) of 0.65 mm penetrates through these two units, and the cell diameter is 77.5 mm. More details of the model can be found in the **section S1** of supporting information. The contact resistances between the nail and electrodes are assumed to be R_1, R_2, and R_3 for top Al, bottom Al and middle Cu layer, respectively. In our simulations, R_3 is kept as a constant (0.163 Ω or 0.02 mΩ cm^2), and the sum of R_1 and R_2 is assumed to be 0.326 Ω or 0.02 mΩ cm^2. The temperature rise due to short circuit and the effect of varying R_1/R_2 are studied (Figures 1b and c). First, it is obvious that the maximum temperature rises fast after nailing and gradually slows down. The heat generation is localized at the nailing point (Figure 1d), since all electronic current accumulates there and dissipates as Joule heating. With homogeneous resistance ($R_1 = R_2$), the maximum temperature rise (ΔT) is only 109 K after 10 s. The heterogeneous R_c has a significant effect on ΔT, When $R_1/R_2 = 3$ and 7, ΔT are 119 and 134 K, respectively, representing an increase of 9.2% and 22.9%, respectively. Moreover, such difference can lead to 44% increase in ΔT when $R_1/R_2 = 40$, which is still possible according to experimental results below. Such heterogeneity has not been considered in past research and it is important to investigate.

2.2. Experimental Measurements of R_c

To quantitatively determine the distribution of R_c in experiments, four probe method is used so that R_c is not mixed with resistances at other electrical connections (see **section S2** in the supporting information for more details). As battery electrodes contain both metal current collector and electrode materials, we measured R_c of three cases separately for full understanding: 1) a nail and a metal current collector itself, 2) a nail and a layer of electrode particle film without a metal substrate, and 3) a nail and an electrode with active material particles coated onto both sides of a metal current collector. Such separated measurements can unveil the dominant factor contributing to the contact resistance. Both dry case and wet case with battery electrolyte of 1 M $LiPF_6$ in EC: DEC (ethylene

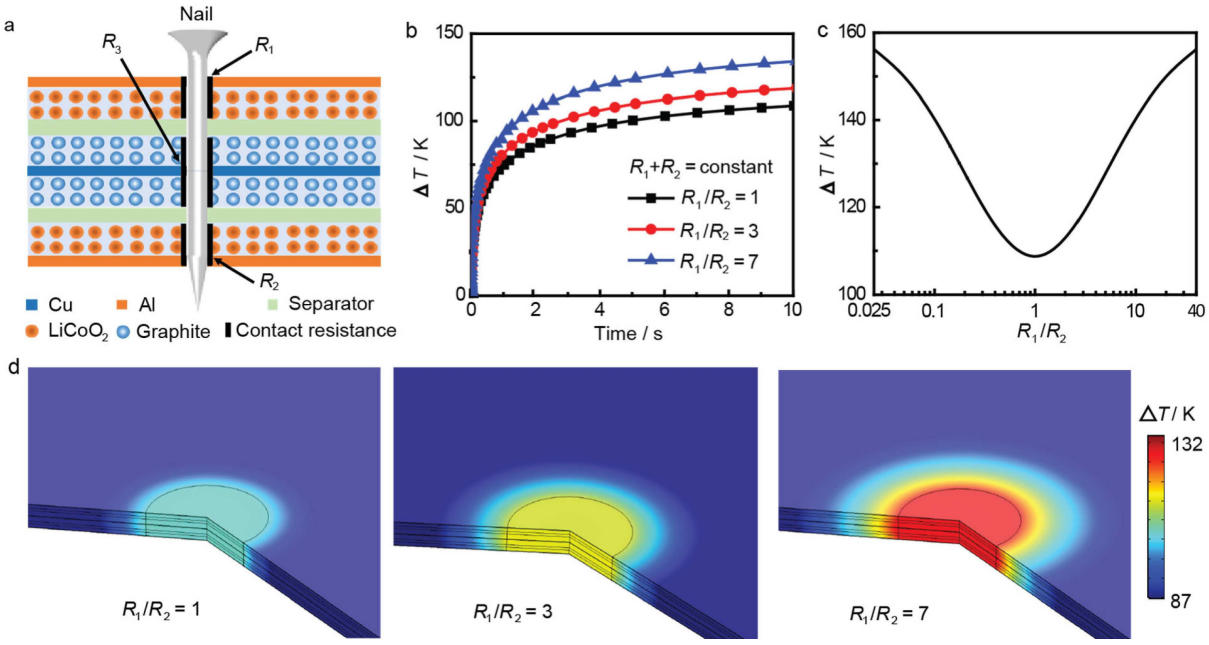

Figure 1. Simulation of temperature rise due to the heterogeneity in contact resistance. (a) The schematic of a two-unit cell for nailing test, assuming $R_1 + R_2 = 0.326$ Ω (or 0.02 mΩ cm^2) and $R_3 = 0.163$ Ω (or 0.02 mΩ cm^2). (b) Maximum temperature increase (ΔT) vs. time at three cases: $R_1/R_2 = 1$, 3, and 7. (c) Maximum temperature increase (ΔT) vs. R_1/R_2. (d) The temperature distribution at 10 s after nail penetration in the three cases in (b).

carbonate/diethyl carbonate in a 1:1 volume ratio) were studied. More experimental details can be found in **sections S3 to S5** of supporting information.

The results show that R_c varies significantly in different cases and have broad distribution in all cases (Figure 2). First, in the wet condition with battery electrolyte, the nail/bare metal current collector has the smallest contact resistance, which are $0.19 \pm 0.12\ \Omega$ ($0.15 \pm 0.09\ m\Omega\,cm^2$) for nail/Al foil and $0.17 \pm 0.12\ \Omega$ ($0.13 \pm 0.09\ m\Omega\,cm^2$) for nail/Cu foil. The smallest/largest resistances observed are 0.002/0.45 Ω (0.002/0.35 $m\Omega\,cm^2$) for nail/Al foil and 0.002/0.42 Ω (0.002/0.33 $m\Omega\,cm^2$) for nail/Cu in ~20 measurements of each case. In contrast, the nail/pure active material film has the highest contact resistance, which is about three orders of magnitude larger than nail/bare metal foil. More specifically, they are $(2.8 \pm 1.4) \times 10^3\ \Omega$ ($5.5 \pm 2.7\ \Omega\,cm^2$) for nail/$LiCoO_2$ active materials and $(2.8 \pm 0.7) \times 10^2\ \Omega$ ($0.55 \pm 0.14\ \Omega\,cm^2$) for nail/graphite active materials. The smallest/largest resistances observed are 660/5887 Ω (1.3/11.6 $\Omega\,cm^2$) for nail/$LiCoO_2$ graphite active materials and 144/466 ΩΩ (0.3/0.9 $\Omega\,cm^2$) for nail/graphite active materials in ~20 measurements of each case. The smaller contact resistance with graphite is likely due to the higher conductivity of graphite (~10^4 S/cm) than $LiCoO_2$ (~1 S/cm).[37]

For real battery electrodes with both active materials and current collector, surprisingly the contact resistance is not the two cases above in parallel, or in series, but a value in the same order of the geometric mean of the two cases above. In real Cu/graphite and Al/$LiCoO_2$ electrode, the contact resistance varies from 0.11 to 4.3 Ω, and 4.0 to 33.1 Ω, respectively. The statistical average and standard deviation are $2.5 \pm 1.5\ \Omega$ ($2.0 \pm 1.2\ m\Omega\,cm^2$) for nail/Cu–graphite electrode and $20.3 \pm 12.4\ \Omega$ ($16.0 \pm 9.7\ m\Omega\,cm^2$) for nail/Al–$LiCoO_2$ electrode respectively. This indicates that in real electrodes with both current collector and active materials, the contact with nail is likely a random

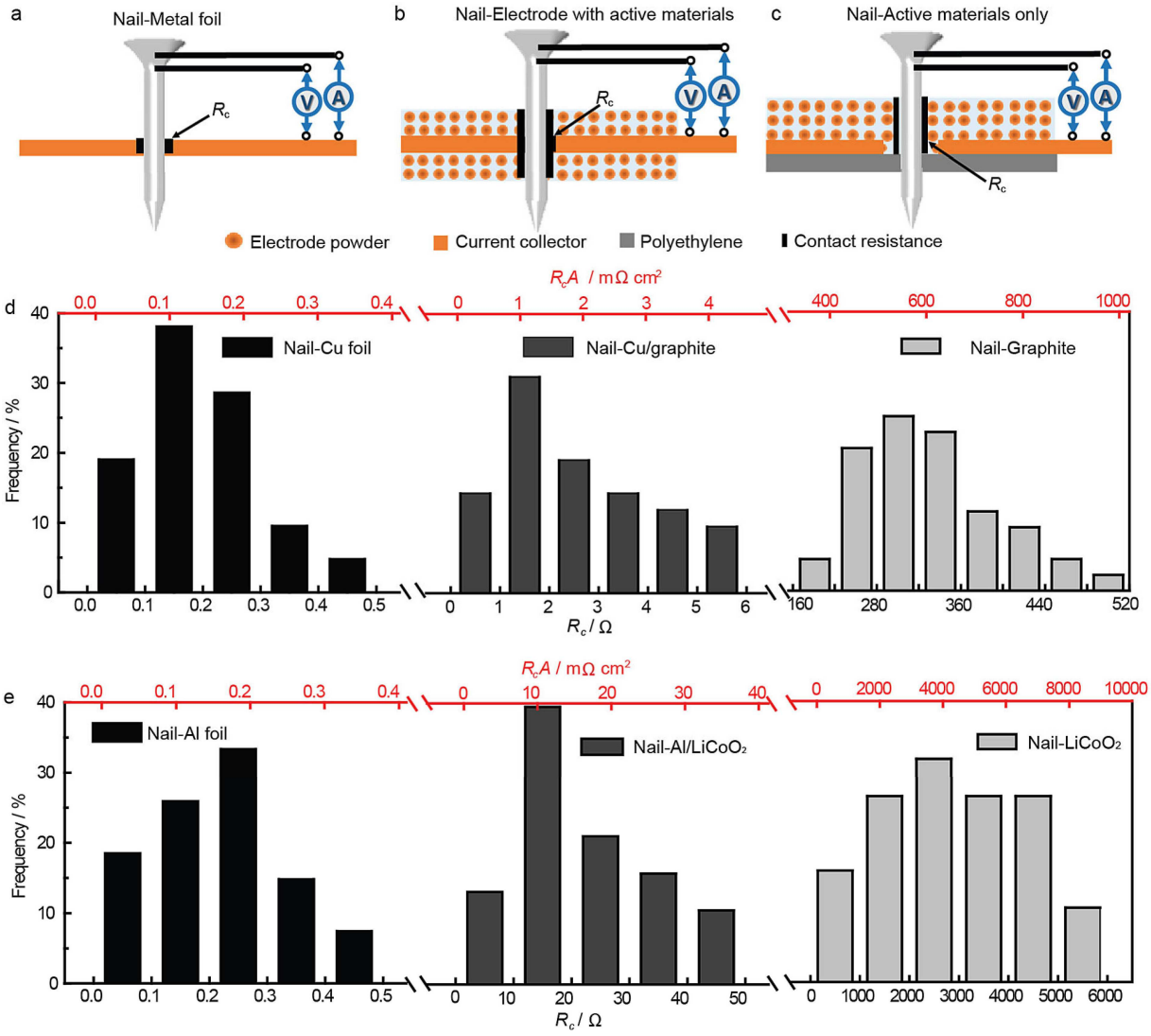

Figure 2. Experimental measurements of the contact resistance (R_c). (a) to (c) Schematic of contact resistance measurement based on the four-probe method (a) with metal substrate, (b) with electrodes and (c) with pure active materials. (d) Distributions of contact resistances for pure Cu foil, Cu foil coated with graphite particles, and graphite particle film themselves under the wet condition. (e) Distributions of contact resistances for the Al foil, Al foil coated with $LiCoO_2$ particles, and $LiCoO_2$ particle film under the wet condition. The diameter of nail is 1.25 mm.

network among metal and active materials, so that it can be described by the Bruggeman's model:[38]

$$\sum_i \delta_i \frac{\sigma_i - \sigma_e}{\sigma_i + (n-1)\sigma_e} = 0 \quad (1)$$

where n is the number of components. δ_i and σ_i are respectively the fraction and the conductivity of each component, and σ_e is the effective conductivity of the medium. When only two phases exist (metal substrate and electrode particle), this model indicates that $\sigma_e = \sqrt{\sigma_1 \sigma_2}$ if the fractions of two components are equal. The calculated R_c were 6.9 Ω and 23 Ω respectively for nail/Cu–graphite electrode and nail/Al–$LiCoO_2$ electrode respectively, which are consistent with our observations.

Since R_c of the nail/graphite interface is one order of magnitude smaller than the nail/$LiCoO_2$ interface, R_c with Cu/graphite is much less than that in Al/$LiCoO_2$. As R_c for Al/$LiCoO_2$ and Cu/graphite are in series for a single repeating unit and the current through these two junctions should be the same, the heat generation in nail penetration localizes at the cathode, as illustrated in **Figure S3**d. This is actually a lucky scenario, since SEI breakdown induced by high temperature is considered as the first step in thermal runaway.[11] The lower R_c at the nail/anode interface indicates less chance for SEI breakdown to happen. Besides the drastic difference in R_c among metal current collectors, active materials, and real electrodes, the broad distribution of R_c means that its heterogeneity across different layers is remarkable in real multi-layer batteries and using the average value instead in modeling will cause significant error in estimating the consequent heat generation and temperature rise, as demonstrated in Figure 1c. Such heterogeneity should be considered in future simulations and experiments.

To understand the contact resistance more comprehensively, we further study effects of the state-of-charge (SOC) on R_c between a nail and active material/current collector bilayer structure in the wet state (Figures S3e and f). It can be seen that R_c is nearly a constant, only decreases slightly with increasing SOC. This is also consistent with the dependence of electrical conductivity of active materials on SOC. For example, Li_xC_6 has higher conductivity of ~10^5 S/cm than pure graphite (~10^4 S/cm).[39] $Li_{0.5}CoO_2$ has higher electrical conductivity of ~10^2 S/cm compared to $LiCoO_2$ (~1 S/cm).[40]

In addition to wet condition with carbonate electrolytes, similar measurements of R_c without the electrolyte were also conducted. As shown in **Figure S5** and **Table S2** (**section S6** of the supporting information), in all cases, R_c is 4~10 times of that in the wet condition. We hypothesize that this is due to the reduced tunneling barrier for electron transport when electrolyte presents, as illustrated in **Figure S6** (**section S7** of the supporting information). At atomistic scale, when surface atoms in nail is angstroms away from the surface atoms in active materials or metal current collectors, tunneling could happen to transport electrons. In the dry state, the barrier to overcome is the energy difference between the fermi level of metal and the vacuum level. In the wet state, the barrier is reduced to the energy difference between the fermi level of metal and the lowest unoccupied molecular orbital (LUMO) of the electrolyte. In standard EC/DEC electrolyte, LUMO is −2.4 eV vs. the vacuum level,[41] so that the tunneling barrier is reduced from ~4.3 to ~1.9 eV when metallic Zn is considered for the nail surface. Therefore, the contact resistance is significantly reduced. Beside the metal nail, the plastic nail was also used in the penetration, we measured the resistance of a dry cell when a plastic nail (D = 1.25 mm) penetrates. Since the nail is sharp, the electrode layer would rupture firstly. Although plastic is insulating, such rupture may cause crack of electrodes and contact between two electrodes. In 20 measurements, most tests give resistance higher than 1 MΩ, indicating no short circuit except three times (**Table S3**), whose contact resistances are 782, 340 and 80239 Ω, respectively. These values are significantly higher than with metal nail, which is 23 ± 17 Ω. Hence, plastic nail is still possible to cause thermal runaway compared to metal nails, but the probability is much less (15% in **Figure S7**). More information can be found in **section S8** of the supporting information.

2.3. Connection Between R_c and Local Stress

To better understand the contact resistance during the penetration process, finite element analysis-based simulation is performed on how local force at the nail/metal foil interface and penetration depth affects R_c. A mechanical-electrical coupled model was built with constitutive relation equation and Electrical contact model coupled by Cooper-Mikic-Yovanovich correlation:[42]

$$h_c = 1.25\sigma_{cont}\frac{m_{asp}}{\sigma_{asp}}\left(\frac{p_{cont}}{H_c}\right)^{0.95} \quad (2)$$

$$\frac{2}{\sigma_{contact}} = \frac{1}{(\sigma_1 \boldsymbol{n}_d)\boldsymbol{n}_d} + \frac{1}{(\sigma_2 \boldsymbol{n}_d)\boldsymbol{n}_d} \quad (3)$$

where h_c is the shrinkage conductivity. $\sigma_{contact}$ is the harmonic mean of the contacting surface conductivities. σ_{asp} is the asperities average height. m_{asp} is the asperities average slope. H_c is the Microhardness. p_{cont} is the contact pressure. $\boldsymbol{n}$ is the normal direction. More details can be found in the **section S9** of supporting information.

The simulation results first show that the magnitude of simulated R_c agrees well with experimental results at the dry condition, both in the range of 0.1–5 Ω, or 0.08–4 mΩ cm^2 (Figure 3a vs. Figure S5), which indicates that the simulation describes the correct physics of contact resistance. Second, the contact resistance is sensitive to the contact force, which decreases with increasing the contact force. This explains why R_c has a broad distribution experimentally, since even small change in local pressure can lead to large change in R_c. For nail with different diameters, although R_c decreases with increasing nail diameter, R_cA changes slightly (Figure 3b), indicating that the nail diameter has a small effect on the area specific contact resistance. Based on these understanding, we finally simulate

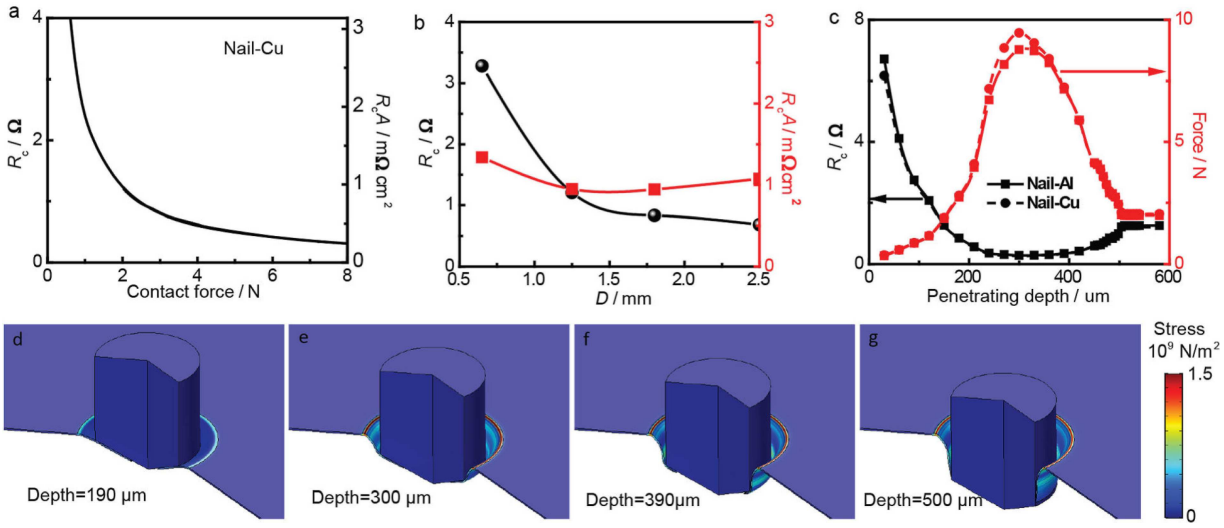

Figure 3. Simulation results of the nail penetrating process. (a) Contact resistance vs. the contact force. (b) Contact resistances vs. the nail radius. (c) Contact resistance vs. the penetrating depth. (d) to (g) Nail and substrate deformation in the penetrating process with the nail diameter of 1.25 mm.

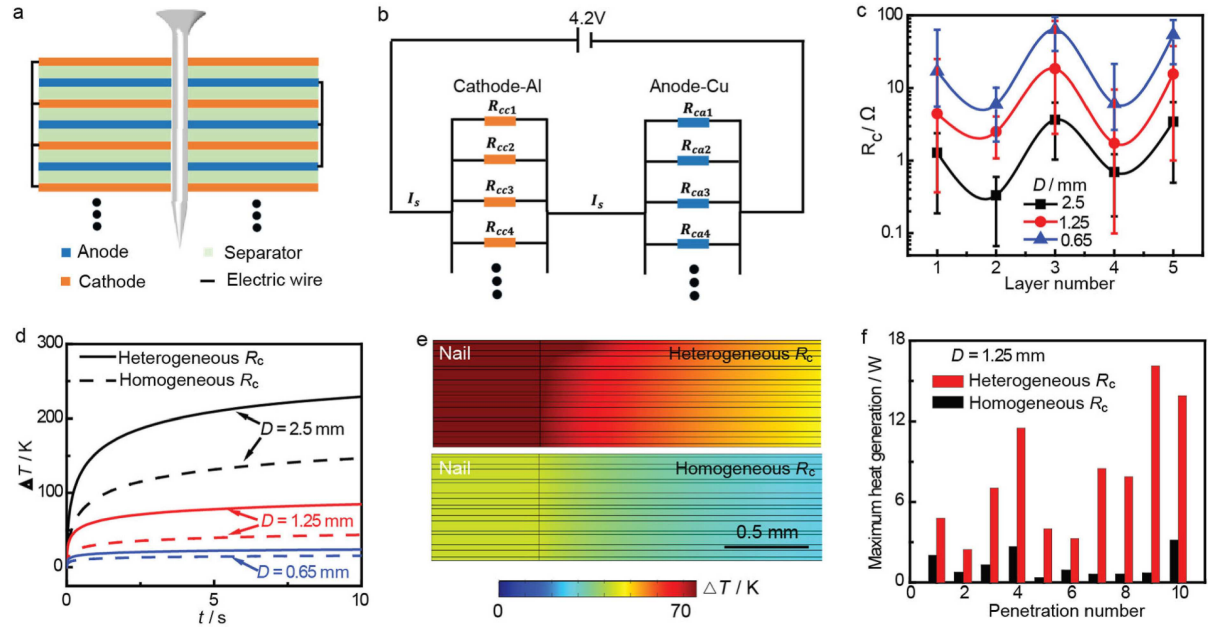

Figure 4. Effects of nail diameter and layer number on R_c and temperature increase. (a) and (b) Schematic diagrams of multilayer stacking cell and equivalent resistance. (c) R_c for different layers and nail diameters. (d) Temperature increase (△T) vs. time for different nail diameters, the solid lines are based on the heterogeneous R_c and the dotted lines are based on homogeneous R_c. (e) maximum heat generation power at ten penetration tests for the heterogeneous and homogeneous R_c cases at the nail diameter of 1.25 mm. (f) temperature distribution at 10 s after nail penetration in the two cases in (e). In the simulation, the stacking cell configuration is used, where all anode layers are connected in parallel, and all cathode electrode layers are connected in parallel.

the evolution in R_c during the penetration process, as shown in Figure 3c. It is clearly that R_c is large at the beginning due to a small contact force. With increasing the penetration depth, the R_c decreases rapidly, which can be attributed to the different contact forces as shown in Figures 3d to g. Then R_c increases slightly due to the decreasing contact force, and finally reaches a steady state when the nail fully penetrates the metal foil without much change of the contact force.

2.4. R_c and Temperature Rise in Multi-Layer Cells

The experimental results above are all based on a single layer stack of one repeating unit of Al/$LiCoO_2$/separator/graphite/Cu. However, most batteries contain multiple repeating units. It is important to understand how the contact resistance varies from layer to layer. To answer this question, a four-repeating-unit cell is constructed and the metal stacking is Al–Cu–Al–Cu–Al (Figure 4a). For top and bottom cathode electrodes, $LiCoO_2$ particles are only coated onto the side facing

the anode. For other electrodes, active materials are coated onto both sides of the current collector. The stacking cell configuration is used, which means that all cathode layers are connected in parallel, and all anode layers are connected in parallel (Figure 4a). Figure 4b shows the schematic diagram of equivalent resistance for such a multilayer stacking cell. The internal resistance of the cell (~0.1 Ω) is neglected as it is much smaller than R_c at different layers (Figure 4c). The calculation details of the internal resistance can be found in the **section S10** of the supporting information. In such a multi-layer cell, R_c for the anode is much smaller than that of the cathode (Figure 4c), which is consistent with results in a single unit cell (Figure 2). For nails with different sizes, the same tendency is observed (Figure 4c). This indicates that diameter does not affect the inhomogeneous distribution of contact resistance. The effect of shape needs further investigation, but as the penetration mechanism is similar to those with circular cross sections, we expect the general trend is the same as what we observed in this manuscript.

Such high heterogeneity in R_c leads to significantly higher heat generation and temperature rise inside the cell compared to the case with homogeneous R_c, as shown in Figures 4d and e, respectively. Take $D = 2.5$ mm as an example, the averaged R_c for each layer was used to simulate the inhomogeneous case, which were 1.28 Ω, 0.33 Ω, 3.67 Ω, 0.70 Ω, and 3.45 Ω from the top cathode to the bottom cathode, respectively. Meanwhile, the average of five R_c above (1.89 Ω) was used for the case with homogeneous R_c. Regarding to temperature rise, ΔT reaches 230 K after 10 s for the inhomogeneous case, while ΔT is only 147 K after 10 s for the uniform case (Figures 4d and e). Similarly, ΔT for the inhomogeneous case are 85 K and 24 K for $D = 1.25$ and 0.65 mm, respectively, while it is only 44 K and 16 K for uniform R_c, which are remarkably lower (Figure 4d). To further validate this, similar calculation was carried out for all ten times of penetrations. The maximum heat generation for the inhomogeneous case is always 300% larger than that of the homogeneous case (Figure 4f). Therefore, it's of great significance to consider such heterogeneity for thermal runaway in batteries. More details of simulation can be found in the supporting information.

In studying the effects of heterogeneous R_c, we notice two correlated interesting and important phenomena. The first one is that the top cathode layer typically has the smallest R_c among all three cathode layers, with a high probability of 60–80% (**Figure S8a**); and thus, R_c for the top layer (averagely 4.4 Ω for $D = 1.25$ mm) is much less than the other two cathode layers (averagely 18.4 and 15.5 Ω). This may arise from that there is no $LiCoO_2$ particles on top of Al, so that the contact behaves more like nail/metal contact instead of metal/electrode contact, and thus R_c is much smaller (Figure S8b). The second phenomenon is that the heat generation of the top cathode layer is more than 213% of the highest one in the rest four layers (Figure 5b).

To understand why this top layer has the highest heat generation and its correlation with the small R_c in this layer, simplified circuit analysis was carried out based on Figure 4b. Here the internal resistance of cells is neglected, since it is much smaller than R_c. Therefore, the heat generation of each layer can be expressed as

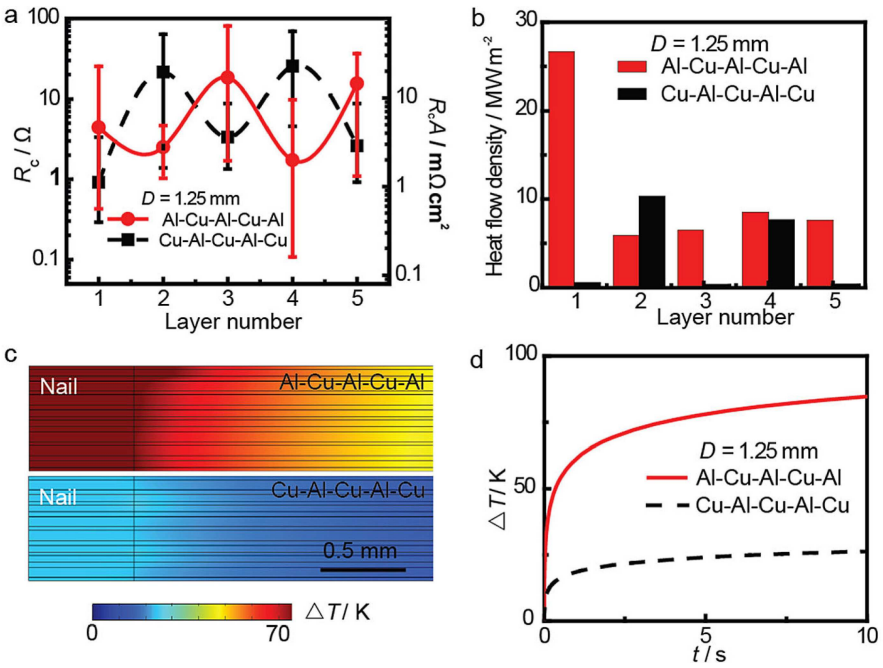

Figure 5. Effects of stacking sequence on R_c and temperature increase. (a) R_c of each layer in two different stacking sequences. (b) Interfacial heat flow density at the nail/electrode contact 10 s after nail penetration in the two cases in (a). (c) Temperature distribution at 10 s after nail penetration in the two cases in (a). (d) Temperature increase (ΔT) vs. time for different stacking sequences, the solid lines are based on the Al–Cu–Al–Cu–Al and the dotted lines are based on the Cu–Al–Cu–Al–Cu. In the simulation, the stacking cell configuration is used, where all anode layers are connected in parallel, and all cathode electrode layers are connected in parallel.

$$P_{cc,i} = \frac{E^2}{(R_{ca} + R_{cc})^2} \cdot \frac{{R_{cc}}^2}{R_{cc,i}} \quad (4)$$

$$P_{ca,i} = \frac{E^2}{(R_{ca} + R_{cc})^2} \cdot \frac{{R_{ca}}^2}{R_{ca,i}} \quad (5)$$

where $P_{cc,i}$ and $P_{ca,i}$ are the heat power for the i layer of the cathode and anode respectively. $R_{cc,i}$ and $R_{ca,i}$are the contact resistance for the i layer of the cathode and anode respectively. $R_{cc} = \left(\sum_n {R_{cc,i}}^{-1}\right)^{-1}$, $R_{ca} = \left(\sum_n {R_{ca,i}}^{-1}\right)^{-1}$, representing the total contact resistance of all cathode and anode in parallel, respectively. Clearly, the maximum $P_{cc,i}$ is the layer with smallest $R_{cc,i}$, or $R_{cc,min}$, which is typically the top layer with a high probability of 80% in experiments (**Figure S8**a). To compare heat generation between cathode and anode layers, the ratio of thermal power in the top cathode ($P_{cc,1}$ or $P_{cc,min}$)) and the j^{th} anode ($P_{ca,j}$) can be expressed as $K = (R_{cc}/R_{ca})^2/\left(R_{cc,\min}/R_{ca,j}\right)$. Therefore, the smallest ratio occurs for the anode layer with smallest $R_{ca,j}$, or $R_{ca,min}$, i.e., $(R_{cc}/R_{ca})^2/\left(R_{cc,\min}/R_{ca,min}\right)$. As $(R_{cc}/R_{ca})^2$ is ~9 averagely and $R_{cc,\min}/R_{ca,min}$ is ~3.4 averagely, K is typically well above 1 so that $P_{cc,max}$ is typically larger than $P_{ca,max}$. Therefore, the top Al layer is most likely to have the highest heat generation. In our experiment, the probability is as large as 60%, far exceeding 20% for random situation (**Table S5** and **Figure S10**c).

2.5. Strategies to Reduce Heat Generation

Based on analysis above, to reduce heat generation, we should first increase $R_{cc} + R_{ca}$, since P is proportional to $(R_{cc} + R_{ca})^2$. As $R_{cc} \gg R_{ca}$, R_{cc} should be increased. We find that a simple method to increase R_{cc} is to replace the cathode (Al) with the anode (Cu) as the outermost layer. In this new sequence, there is no cathode layer with active materials only on one side of Al. Therefore, R_{cc} is increased dramatically. The average R_{cc} among ten tests increases from 0.9 Ω in Al–Cu–Al–Cu–Al to 8.7 Ω in Cu–Al–Cu–Al–Cu, and a statistics is presented in Figure S10 and Table S5. Meanwhile, although the average R_{ca} among ten tests decreases from 0.6 Ω in Al–Cu–Al–Cu–Al to 0.4 Ω in Cu–Al–Cu–Al–Cu (**Figure S11**), it has little effect on $R_{cc} + R_{ca}$.

The increase of $(R_{cc} + R_{ca})^2$also overwhelms changes in ${R_{cc}}^2/R_{cc,\min}$ and ${R_{ca}}^2/R_{ca,\min}$ in **equations (4)** and **(5)**. Hence, the maximum heat generation in Cu–Al–Cu–Al–Cu also occurs in the cathode layer with $R_{cc,\min}$ in Figure S10f, which is only ~39% of that in the Al–Cu–Al–Cu–Al case. For example, when the average R_c for each layer in ten tests are used, the highest single-layer heat generation is reduced from 26.7 MWm^{-2} to 10.0 MWm^{-2} at the contact interface (Figure 5b), and the total heat generation power is reduced from 4.5 W to 1.5 W. Consequently, the largest temperature rise in Cu–Al–Cu–Al–Cu is only 26 °C, much less than 85 °C in Al–Cu–Al–Cu–Al, which can be attributed to the much higher $R_{cc} + R_{ca}$ in Cu–Al–Cu–Al–Cu (9.1 Ω) than that in Al–Cu–Al–Cu–Al (1.5 Ω). More details can be found in **Section S13** of the supporting information.

We further investigated whether this strategy can be extended to even thicker cells. For a cell with eight repeating units, the one with anode as outermost layers shows a much lower temperature rise (29 °C) compared to that with cathode as outermost layer (75 °C) (**Figure S12**a). Such results demonstrate the importance to deeply understand the heterogeneity of contact resistance, which leads to the better sequence for cell stacking and reduced temperature rise: anode as the outermost layer.

3. Conclusions

In summary, we have experimentally measured the short-circuit contact resistance in nail penetration for the first time, to the best of our knowledge. The contact resistance between a nail and a battery electrode is in the same order of the geometric mean of nail/active material and nail/metal substrate, suggesting a random connection network model. The contact resistance also shows wide distribution and large fluctuation, such as 2.5 ± 1.5 Ω for nail/graphite on Cu foil, and 20.3 ± 12.4 Ω for nail/$LiCoO_2$ on Al foil. Such large heterogeneity is likely to arise from local stress, to which contact resistance is sensitive, as supported by finite element analysis-based simulations. Understanding and measuring such heterogeneity is critical for investigating thermal runaway in batteries, since the inhomogeneous contact resistance leads to significantly higher temperature rise in thermal runaway of a battery. The dependence of contact resistance on various factors, such as nail dimension, electrode layer numbers, electrolyte content and layer sequences, are also investigated to obtain a comprehensive understanding. Finally, we show that having anode as the outermost layer can significantly reduce heat generation during nail penetration, compared to that with cathode as the outermost layer, which provides guidance to enhance battery safety.

Experimental Section

Materials: The battery electrolyte of 1 M $LiPF_6$ in ethylene carbonate/diethyl carbonate (EC:DEC in a 1:1 volume ratio) was purchased from Gotion Inc., and used as received. The solvent N-Methyl-2-pyrrolidone (NMP) and Aluminized pouch bags and (Sigma-Aldrich). polyvinylidene fluoride (PVDF), $LiCoO_2$ and graphite powders were purchased from MTI Corporation. Carbon black (C65) was from IMERYS. Nails (diameter: 2.5 mm, 1.25 mm and 0.65 mm) were purchased from McMaster-Carr. Commercial $LiCoO_2$ cathode and graphite anode were provided by Custom Electronics Inc.

Contact resistance measurement: The four-probe method was used to measure the contact resistance using an electrochemical workstation (Bio-logic SP-50) to record the current-voltage after the nail penetration. For measuring the contact resistance between the nail and active materials, active materials were coated onto a metal foil with a hole in the center. Then nail was inserted into the hole. Therefore, the nail did not contact with metal foils, but meanwhile, the resistance of active materials themselves was negligible. For measuring contact resistance at different state-of-charges, the electrode was charged to the target *SOC* first in a pouch cell. Then the cell was dissembled and the charged electrode was sealed in

another cell for four point measurement. Hence, the electrical signal would not be interfered by electrochemical cell voltage. More details can be found in the supporting information.

Short circuit simulation: The internal-shorting-induced Joule heating behavior of batteries was simulated by COMSOL Mutiphysics 5.3a. One standard cell consisted of a graphite anode and a $LiCoO_2$ cathode with $LiPF_6$ electrolyte in 3:7 EC:EMC solvent. Al and Cu foils were used on the positive and negative current collectors, respectively. The initial cell voltage was 4.2 V and the Cu foil was grounded. The rest of the outer boundaries was set to be electrically insulated. The internal short circuit was induced by a stainless steel nail penetrates through the center of the battery. More details can be found in the supporting information.

Mechanical deformation simulation for the nail penetration process: The contact resistance from the mechanical crash of the nail penetration process was simulated by using a coupled 3D Solid Mechanics and AC/DC modules by COMSOL Mutiphysics 5.3a. The foil is deformed by a nail with a prescribed vertical displacement which is ramped linearly. An isotropic elastoplastic material with user-defined isotropic hardening and large plastic strain formulation is used to characterize the plastic deformation of the Cu or Al foils. Static Hertz contact model were used to calculate the electric contact resistance. More details can be found in the supporting information.

Acknowledgements

M.C. and Q.Y. contributed equally to this work. Y.Y. acknowledges support from startup funding by Columbia University. This work is supported by the NSF-MRSEC program through Columbia in the Center for Precision Assembly of Superstratic and Superatomic Solids (DMR-1420634) and sponsored by the China Scholarship Council (CSC) graduate scholarship.

Conflict of Interest

The authors declare no conflict of interest.

Keywords: nail penetration · contact resistance · short circuit · batteries · electrodes

[1] Z. Gao, H. Sun, L. Fu, F. Ye, Y. Zhang, W. Luo, Y. Huang, *Adv. Mater.* **2018**, *30*, 1–27.
[2] H. Zhai, P. Xu, M. Ning, Q. Cheng, J. Mandal, Y. Yang, *Nano Lett.* **2017**, *17*, 3182–3187.
[3] J. B. Goodenough, K. S. Park, *J. Am. Chem. Soc.* **2013**, *135*, 1167–1176.
[4] Z. J. Zhang, P. Ramadass, W. Fang, in *Lithium-Ion Batter. Adv. Appl.*, **2014**, pp. 409–435.
[5] Q. Wang, P. Ping, X. Zhao, G. Chu, J. Sun, C. Chen, *J. Power Sources* **2012**, *208*, 210–224.
[6] Y. Yang, X. Huang, Z. Cao, G. Chen, *Nano Energy* **2016**, *22*, 301–309.
[7] R. Marom, S. F. Amalraj, N. Leifer, D. Jacob, D. Aurbach, *J. Mater. Chem.* **2011**, *21*, 9938–9954.
[8] V. Etacheri, R. Marom, R. Elazari, G. Salitra, D. Aurbach, *Energy Environ. Sci.* **2011**, *4*, 3243–3262.
[9] G. Qian, B. Zhu, X. Liao, H. Zhai, A. Srinivasan, N. J. Fritz, Q. Cheng, M. Ning, B. Qie, Y. Li, *Adv. Mater.* **2018**, *30*, 1704947.
[10] M. Hao, J. Li, S. Park, S. Moura, C. Dames, *Nat. Energy* **2018**, *3*, 899–906.
[11] X. Feng, M. Ouyang, X. Liu, L. Lu, Y. Xia, X. He, *Energy Storage Mater.* **2018**, 246–267.
[12] Z. Chen, P. C. Hsu, J. Lopez, Y. Li, J. W. F. To, N. Liu, C. Wang, S. C. Andrews, J. Liu, Y. Cui, *Nat. Energy* **2016**, *1*, 15009.
[13] L. Xia, D. Wang, H. Yang, Y. Cao, X. Ai, *Electrochem. Commun.* **2012**, *25*, 98–100.
[14] H. Wu, D. Zhuo, D. Kong, Y. Cui, *Nat. Commun.* **2014**, *5*, 1–6.
[15] P. Bai, J. Li, F. R. Brushett, M. Z. Bazant, *Energy Environ. Sci.* **2016**, *9*, 3221–3229.
[16] Y. Li, Y. Li, A. Pei, K. Yan, Y. Sun, C. L. Wu, L. M. Joubert, R. Chin, A. L. Koh, Y. Yu, *Science (80-.).* **2017**, *358*, 506–510.
[17] X. Wang, M. Zhang, J. Alvarado, S. Wang, M. Sina, B. Lu, J. Bouwer, W. Xu, J. Xiao, J. G. Zhang, *Nano Lett.* **2017**, *17*, 7606–7612.
[18] M. S. Kim, J.-H. Ryu, Deepika, Y. R. Lim, I. W. Nah, K.-R. Lee, L. A. Archer, W. Il Cho, *Nat. Energy* **2018**, *3*, 889–898.
[19] R. Bhattacharyya, B. Key, H. Chen, A. S. Best, A. F. Hollenkamp, C. P. Grey, *Nat. Mater.* **2010**, *9*, 504–510.
[20] Q. Cheng, L. Wei, Z. Liu, N. Ni, Z. Sang, B. Zhu, W. Xu, M. Chen, Y. Miao, L.-Q. Chen, *Nat. Commun.* **2018**, *9*, 2942.
[21] K. J. Harry, D. T. Hallinan, D. Y. Parkinson, A. A. MacDowell, N. P. Balsara, *Nat. Mater.* **2014**, *13*, 69–73.
[22] R. Zhao, J. Liu, J. Gu, *Appl. Energy* **2016**, *173*, 29–39.
[23] T. D. Hatchard, S. Trussler, J. R. Dahn, *J. Power Sources* **2014**, *247*, 821–823.
[24] B. Mao, H. Chen, Z. Cui, T. Wu, Q. Wang, *Int. J. Heat Mass Transfer* **2018**, *122*, 1103–1115.
[25] T. Yokoshima, D. Mukoyama, F. Maeda, T. Osaka, K. Takazawa, S. Egusa, S. Naoi, S. Ishikura, K. Yamamoto, *J. Power Sources* **2018**, *393*, 67–74.
[26] C. S. Kim, J. S. Yoo, K. M. Jeong, K. Kim, C. W. Yi, *J. Power Sources* **2015**, *289*, 41–49.
[27] B. Liu, Y. Jia, J. Li, S. Yin, C. Yuan, Z. Hu, L. Wang, Y. Li, J. Xu, *J. Mater. Chem. A* **2018**, *6*, 21475–21484.
[28] K. C. Chiu, C. H. Lin, S. F. Yeh, Y. H. Lin, K. C. Chen, *J. Power Sources* **2014**, *251*, 254–263.
[29] W. Zhao, G. Luo, C.-Y. Wang, *J. Electrochem. Soc.* **2015**, *162*, A1352–A1364.
[30] D. P. Finegan, B. Tjaden, T. M. M. Heenan, R. Jervis, M. Di Michiel, A. Rack, G. Hinds, D. J. L. Brett, P. R. Shearing, *J. Electrochem. Soc.* **2017**, *164*, A3285–A3291.
[31] R. Zhao, J. Liu, J. Gu, *Energy* **2017**, *123*, 392–401.
[32] B. Liu, S. Yin, J. Xu, *Appl. Energy* **2016**, *183*, 278–289.
[33] X. Feng, J. Sun, M. Ouyang, F. Wang, X. He, L. Lu, H. Peng, *J. Power Sources* **2015**, *275*, 261–273.
[34] E. Sahraei, J. Campbell, T. Wierzbicki, *J. Power Sources* **2012**, *220*, 360–372.
[35] S. Wilke, B. Schweitzer, S. Khateeb, S. Al-Hallaj, *J. Power Sources* **2017**, *340*, 51–59.
[36] W. Zhao, G. Luo, C.-Y. Wang, *J. Electrochem. Soc.* **2014**, *162*, A207–A217.
[37] M. Park, X. Zhang, M. Chung, G. B. Less, A. M. Sastry, *J. Power Sources* **2010**, *195*, 7904–7929.
[38] https://en.wikipedia.org/wiki/effective_medium_approximations.
[39] S. Basu, C. Zeller, P. J. Flanders, C. D. Fuerst, W. D. Johnson, J. E. Fischer, *Mater. Sci. Eng.* **1979**, *38*, 275–283.
[40] Y. Takahashi, N. Kijima, K. Tokiwa, T. Watanabe, J. Akimoto, *J. Phys. Condens. Matter* **2007**, *19*, 0–12.
[41] J. B. Goodenough, Y. Kim, *Chem. Mater.* **2010**, *22*, 587–603.
[42] N. Pandey, I. Jain, S. Reddy, N. P. Gulhane, *AIP Conf. Proc.* **2018**, *1966*, 020017.

Manuscript received: June 5, 2019
Accepted manuscript online: June 28, 2019
Version of record online: July 18, 2019